Measured Effects of Diacylglycerol on Structural and Elastic Properties of Phospholipid Membranes

S. Leikin,* M. M. Kozlov,# N. L. Fuller,§ and R. P. Rand§

*Laboratory of Structural Biology, Division of Computer Research and Technology, National Institutes of Health, Bethesda, Maryland 20892 USA; #Department of Physiology and Pharmacology, Sackler Faculty of Medicine, Tel Aviv University, Ramat-Aviv 69978 Israel; and §Department of Biological Sciences, Brock University, St. Catharines, Ontario L2S 3A1 Canada

ABSTRACT Diacylglycerol, a biological membrane second messenger, is a strong perturber of phospholipid planar bilayers. It converts multibilayers to the reverse hexagonal phase (H_{II}), composed of highly curved monolayers. We have used x-ray diffraction and osmotic stress of the H_{II} phase to measure structural dimensions, spontaneous curvature, and bending moduli of dioleoylphosphatidylethanolamine (DOPE) monolayers doped with increasing amounts of dioleoylglycerol (DOG). The diameter of the H_{II} phase cylinders equilibrated in excess water decreases significantly with increasing DOG content. Remarkably, however, all structural dimensions at any specific water/lipid ratio that is less than full hydration are insensitive to DOG. By plotting structural parameters of the H_{II} phase with changing water content in a newly defined coordinate system, we show that the elastic deformation of the lipid monolayers can be described as bending around a pivotal plane of constant area. This dividing surface includes 30% of the lipid volume independent of the DOG content (polar heads and a small fraction of hydrocarbon chains). As the mole fraction of DOG increases to 0.3, the radius of spontaneous curvature defined for the pivotal surface decreases from 29 Å to 19 Å, and the bending modulus increases from ~11 to 14 (± 0.5) kT. We derive the conversion factors and estimate the spontaneous curvatures and bending moduli for the neutral surface which, unlike the pivotal plane parameters, are intrinsic properties that apply to other deformations and geometries. The spontaneous curvature of the neutral surface differs from that of the pivotal plane by less than 10%, but the difference in the bending moduli is up to 40%. Our estimate shows that the neutral surface bending modulus is ~9kT and practically does not depend on the DOG content.

INTRODUCTION

The production of diacylglycerols (DGs) in membranes from the stimulus-induced activation of phospholipases (Berridge, 1984) is part of a ubiquitous transmembrane signaling system. DG results in the activation of protein kinase C (Nishizuka, 1984) and of a variety of phospholipases (Dawson et al., 1984). Its production is also tightly correlated with the fusion of membranes in different systems (Allan and Michell, 1975; Wakelam, 1983; Whitaker and Aitchison, 1985).

How does DG modify lipid-protein interactions in membranes? And what is its role in the topological rearrangements in membrane fusion? DG is a strongly hydrophobic molecule that shows little interaction with water and perturbs phospholipid planar bilayers. As shown in NMR studies, DG modifies the conformation both of phospholipid headgroups (Goldberg et al., 1995) and of phospholipid hydrocarbon chain packing (Goldberg et al., 1994). It can convert phospholipid multibilayers into nonbilayer structures, especially into the reverse hexagonal phase (H_{II}) (Das and Rand, 1986), but also into cubic phases if cholesterol is present (Nieva et al., 1995).

We aim to define diacylglycerol's structural and mechanical effects in phospholipids. We use x-ray diffraction and osmotic stress of the H_{II} phase to measure DG's effect on structural dimensions, spontaneous curvatures, and bending moduli of dioleoylphosphatidylethanolamine layers. This is based on a new, more accurate recipe for data analysis. We discuss ambiguities in definitions of spontaneous curvature and of bending modulus that become important for highly curved monolayers in the H_{II} phase. In the Appendix we consider the two most common definitions, those based on a pivotal plane and on a neutral surface of bending. We derive a simple relationship between them that is applicable to monolayer deformations associated with the H_{II} phase hydration.

This paper is divided into two parts. In the main text we follow recipes for data analysis, foregoing the details of some theoretical issues. All rigorous definitions, derivations, and more complex issues are discussed in the Appendix. We refer to them in the main text as needed.

MATERIALS, METHODS, AND ANALYSIS

Sample preparation and x-ray diffraction

Synthetic L-α-dioleoylphosphatidylethanolamine (DOPE) and dioleoylglycerol (DOG) were purchased from Avanti Polar Lipids (Birmingham, AL) and used without further purification. The lipid was checked for impurities by thin-layer chromatography and judged to be at least 98% pure.

Structural dimensions of the H_{II} phases were measured at different degrees of lipid hydration and with varying osmotic stress, as described by

Received for publication 19 March 1996 and in final form 1 August 1996.

Address reprint requests to Dr. Sergey Leikin, National Institutes of Health, Bldg. 12A, Rm. 2041, Bethesda, MD 20892. Tel.: 301-496-1121; Fax: 301-496-2172; E-mail: leikin@helix.nih.gov.

0006-3495/96/11/2623/10 $2.00

Rand and Fuller (1994) and Rand et al. (1990). Briefly, dry lipid was prepared by mixing chloroform solutions of the individual lipid species, drying first by rotary evaporation and finally under vacuum. Dry lipid was then hydrated by weighing into small bottles, adding known weights of 2 mM *N*-tris-(hydroxymethyl) methyl-2-aminoethanesulfonic acid (TES) buffer (pH 7.4) or excess amounts of polyethylene glycol solutions of known osmotic pressure Π, and sealing and equilibrating the samples in the dark at room temperature for 48 h. Before mounting, each sample was combined with some powdered teflon as an x-ray calibration standard and then sealed between mica windows 1 mm apart.

X-ray diffraction was used to characterize the structures formed by the hydrated lipid. The $CuK_{\alpha 1}$ line (λ = 1.540 Å), from a Rigaku rotating anode generator, was isolated with a bent quartz crystal monochromator, and diffraction patterns were recorded photographically using Guinier x-ray cameras operating in vacuo. Temperature was controlled with thermoelectric elements to approximately ±0.5°C. All samples formed hexagonal phases characterized by at least three x-ray spacings bearing ratios to the dimension of the first order, d_{hex}, of 1, $1/\sqrt{3}$, $1/\sqrt{4}$, $1/\sqrt{7}$, $1/\sqrt{9}$, $1/\sqrt{12}$, etc., yielding d_{hex} with a measuring error of ±0.1 Å. Sample-to-sample variations in lattice dimensions, which include all experimental errors, cover a maximum range of ±0.5 Å.

Structure analysis

H_{II} phases are two-dimensional hexagonal lattices formed by the axes of indefinitely long and parallel regular prisms (Fig. 1). Water cores, centered on the prism axes, are lined with the lipid polar groups, and the rest of the lattice is filled with the hydrocarbon chains. Here the cross-sectional shape of the water core prism within that lattice is assumed to be circular, although it has been shown that that cross section can be distorted from circularity (Turner and Gruner, 1992).

For a hexagonal phase of known composition, the measured lattice can be divided into compartments, as shown in Fig. 1, each containing defined volume fractions of the lipid and water. This volume average division follows the method originally introduced by Luzzati (e.g., see Luzzati and Husson, 1962) and depends only on a knowledge of the specific volumes of the molecular components and on the assumption of their linear addition. The specific volumes for lipid components of the lattice are given in Table 1.

In particular, we separate the water and lipid compartments by introducing an idealized cylindrical interface that encloses a volume equal to the volume of water in the H_{II} phase (Fig. 1). We then use it for data analysis as if all the water is inside and all the lipid is outside of this cylinder. We refer to the surface of this cylinder as the Luzzati plane (in fact, this is the definition for a Gibbs dividing surface of zero surface excess of water and lipid; see Appendix).

The radius of the water cylinder, R_w, is related to the first-order Bragg spacing in the hexagonal phase, d_{hex}, and to the volume fraction of water in the sample, ϕ_w, as follows:

$$R_w = d_{hex}\sqrt{\frac{2\phi_w}{\pi\sqrt{3}}}. \quad (1)$$

The area per lipid molecule at the Luzzati plane is given by

$$A_w = \frac{2\phi_w V_l}{(1-\phi_w)R_w}, \quad (2)$$

where V_l is the volume of a lipid molecule. These equations determine the Luzzati plane parameters, using d_{hex}, measured in the x-ray experiment, and ϕ_w, calculated from the weight fraction of water in the samples using specific molecular volumes given in Table 1.

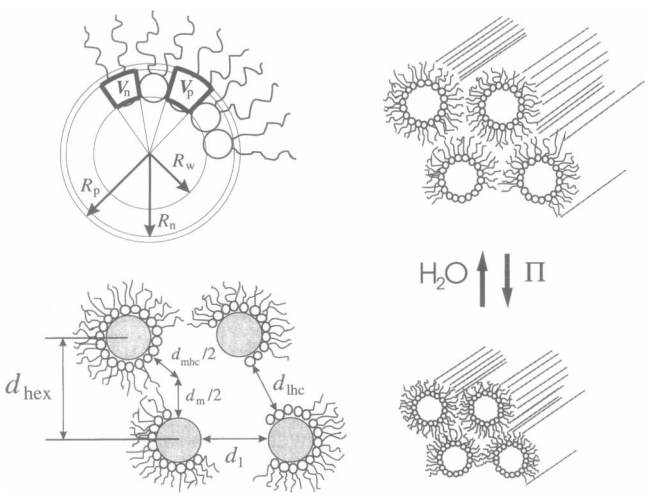

FIGURE 1 Schematic diagram of the hexagonal phase structure showing dimensions determined and used in the structural and energetic analysis. X-ray diffraction gives d_{hex}. Sample composition and component densities give the volume fractions of water and lipid, both polar and hydrocarbon portions. From those are derived the structural dimensions shown. Dimension changes are effected by osmotically or gravimetrically controlling water content, as illustrated on the right. The Luzzati plane is one that divides the lattice into two parts, one that contains all and only the lipid volume, the other only the water volume, giving cylinder radius R_w. The radius of any other dividing surface within the cylindrical monolayer is determined by the portion (V) of the total (V_l) molecular lipid volume that is included in it. For DOG/DOPE mixtures we use an effective volume that includes DOPE and the mole fraction of DOG. The experimental results show that there exists a pivotal surface at R_p that includes V_p, the area of which does not change with water content. We use a neutral surface at R_n that includes V_n to relate these measurements to intrinsic elastic properties of the monolayer. We calculate equivalent bilayer and hydrocarbon chain thickness in the interaxial (d_l, d_{lhc}) and interstitial (d_m, d_{mhc}) directions as defined by Rand and Fuller (1994).

Elastic energy of the hexagonal phase

In principle, the curvature and molecular areas at the Luzzati plane can be used directly to characterize the elastic energy of monolayer deformation. However, to simplify the analysis, the H_{II} phase is usually described in terms of curvature and molecular area on either of two other cylindrical surfaces lying inside the lipid monolayer (Fig. 1): 1) a neutral surface of bending where the bending and stretching (compression) deformations are energetically uncoupled (Kozlov and Winterhalter, 1991a,b); 2) a pivotal

TABLE 1 Specific volumes for different lipid components in DOPE/DOG mixtures

	Mol. wt.	Partial specific volume	Volume (Å^3)
DOPE	744	1.00	1235
DOG	621	1.08	1116
DOPE polar group	269	0.699	312
DOG polar group	146	0.796	193
DOPE/DOG chains	475	1.17	923

The specific volumes of many phospholipids have been measured directly. Here those of DOPE and water have both been taken as 1.00. The specific volume of the DOG polar group was derived from glycerol density (Lide, 1994). The specific volume of melted hydrocarbon chains of the lipids was derived as 1.17 cm^3/g (see Rand and Parsegian, 1989, for a detailed discussion of molecular densities). The polar groups are defined as including all polar moieties, including the carbonyls at the polar group ends of the attached fatty acid hydrocarbon chains.

plane where the molecular area remains constant (Rand et al., 1990). Here we analyze the experimental data using the pivotal plane, because its position can be found from the data with much higher accuracy. For comprehensive discussion including the related approximations, rigorous definitions, existence criteria, and the relationship between the pivotal and neutral plane parameters, see the Appendix.

By using the radius of curvature at the pivotal plane, R_p, the elastic free energy, F, of the hexagonal phase (normalized per lipid molecule) can be approximated by the energy of bending (Helfrich, 1973; Kirk et al., 1984),

$$F = \frac{1}{2} k_{cp} A_p \left(\frac{1}{R_p} - \frac{1}{R_{0p}} \right)^2, \quad (3)$$

where k_{cp} is the monolayer bending modulus, and A_p and R_{0p} are the molecular area and the spontaneous radius of curvature at the pivotal plane. The goal of the measurement is to find the position of the pivotal plane, the spontaneous curvature, molecular area, and bending moduli for different DOPE/DOG mixtures.

The recipe

The molecular area A and radius of curvature R at any cylindrical dividing surface, separated by a volume V per lipid molecule from the Luzzati plane (Fig. 1), are given by

$$A^2 = A_w^2 + 2V\frac{A_w}{R_w} \quad \text{or} \quad A = A_w\sqrt{1 + \frac{1-\phi_w}{\phi_w}\frac{V}{V_l}} \quad (4)$$

$$R = R_w\sqrt{1 + \frac{1-\phi_w}{\phi_w}\frac{V}{V_l}}. \quad (5)$$

These equations are based purely on geometry. They are valid for any cylindrical dividing surface inside the monolayer, including the pivotal plane.

We verify whether the system has a well-defined pivotal plane and determine its location by plotting A_w^2 versus A_w/R_w. Indeed, rewriting Eq. 4 in the form

$$A_w^2 = A_p^2 - 2V_p\frac{A_w}{R_w}, \quad (6)$$

we find that if the plot is a straight line, the system has a dividing surface of constant area, which is the pivotal plane. We determine its location (V_p, the volume separating this plane and the Luzzati plane) and the molecular area (A_p) from the slope and the intercept of the plot.

From the value of V_p we calculate the radii of curvature (R_p) at the pivotal plane by using Eq. 5. We use these radii and follow the previously suggested recipe (Gruner et al., 1986; Rand et al., 1990) for determining the elastic parameters of the lipid mixture from osmotic stress experiments. Specifically, comparing the elastic energy given by Eq. 3 with the osmotic work done by the osmotic stress (Π), we find the following relationship:

$$\Pi R_p^2 = 2k_{cp}\left(\frac{1}{R_p} - \frac{1}{R_{0p}}\right). \quad (7)$$

The plot of (ΠR_p^2) versus $(1/R_p)$ gives, simultaneously from the slope and the intercept, the monolayer bending modulus (k_{cp}) and the spontaneous curvature ($1/R_{0p}$) (Gruner et al., 1986; Rand et al., 1990).

We note in particular that linearity of the diagnostic A_w^2 versus A_w/R_w plot should not be taken for granted. For large changes in curvature, the plot may be nonlinear, and a pivotal plane associated with a certain fixed place inside the monolayer may not exist. Strictly speaking, under most circumstances this would be the expected behavior (see Appendix). However, despite large changes in curvature, this plot is linear for all DOPE/DOG mixtures we use in this work, so that the fixed pivotal plane does exist. For the sake of simplicity, in the main text of the paper we just deal with the properties of this pivotal plane without concerning ourselves with the question of why it exists. In the Appendix we discuss the latter issue, which we believe is nontrivial and very important.

RESULTS

Gravimetric and osmotic stress data

Fig. 2 shows the measured hexagonal dimension, d_{hex}, of the gravimetrically prepared samples of DOPE and of four different mixtures of DOPE and DOG. The final equilibrium dimension in excess water, the degree of swelling of the hexagonal phase, clearly decreases with increasing amounts of DOG. Remarkably, in less than excess water, for each mixture, the dimension of the hexagonal lattice does not change detectably with DOG content. Consequently, all of the data of Fig. 2 *a* for less than excess water are pooled into one least-squares fit line, as plotted in Fig. 2 *b*, to determine the dependence of the volume fraction of water (ϕ_w) on the hexagonal spacing (d_{hex}), which is used for analysis of the osmotic stress data. We use the intersection of that line with the averaged maximum dimension of the hexagonal phase to determine the water content of the

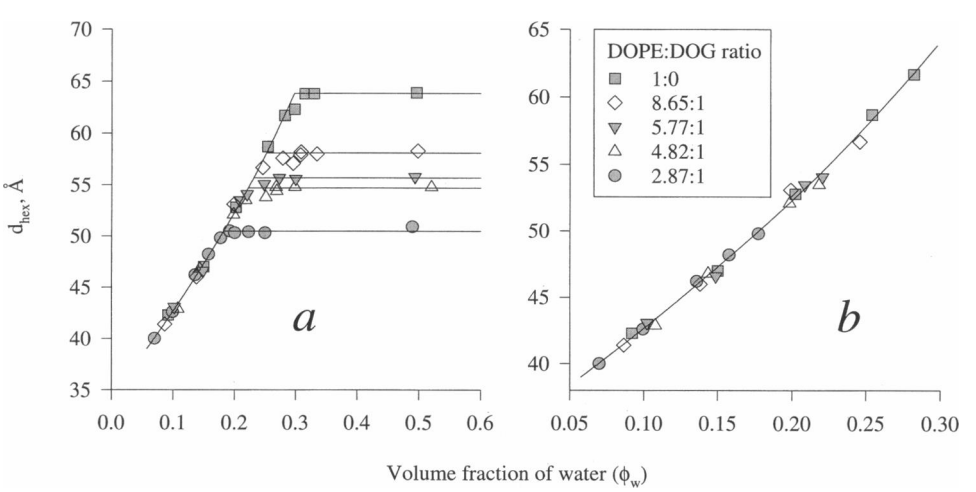

FIGURE 2 Experimental data relating the first-order x-ray spacing of the lamellar phase, d_{hex}, and the volume fraction of water (ϕ_w) in the sample. Increasing the mole ratio DOG/DOPE results in lower fully hydrated lattice dimensions, indicated by the horizontal lines (*a*). This limiting dimension was determined as described in the text. The lattice dimension is remarkably invariant with changing DOG content for all samples at less than full hydration (*b*). The fitted $\phi_w(d_{hex})$ solid line at less than full hydration (*a* and *b*) is used as a calibration to calculate ϕ_w from measured d_{hex} in osmotic stress experiments.

maximally swelled hexagonal phase of each mixture. Several other structural parameters of the fully hydrated lipids are collected in Table 2.

The lattice dimensions of osmotically stressed hexagonal phases of DOPE and five different mixtures of DOPE and DOG are shown in Fig. 3. As DOG content increases, the lattices start from ever smaller sizes. As they are osmotically shrunk they appear to converge at high pressures, or small water content. The composition of each of these phases (ϕ_w) is determined from the $\phi_w(d_{hex})$ dependence (Fig. 2 *b*) obtained by fitting the gravimetric data. The radius of curvature and the molecular area at the Luzzati plane (R_w, A_w) are determined from Eqs. 1 and 2.

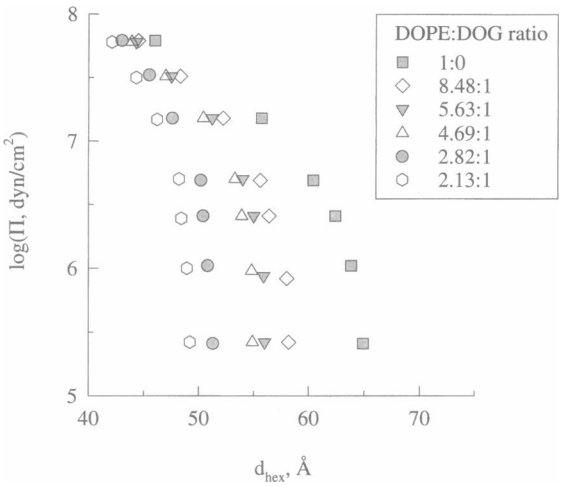

FIGURE 3 Experimental data relating the osmotic pressure, Π, of the equilibrating solutions and the resulting lattice dimension d_{hex}. With increasing mole ratio DOG/DOPE, the lattices start from ever decreasing lattice dimension at low pressures but converge toward the higher pressures.

Data analysis

To standardize the analysis of DOPE/DOG mixtures, we introduce the notion of an effective molecule that is DOPE + xDOG, where $x < 1$ is the molar ratio of DOG to DOPE in the sample. The volume of the effective molecule is

$$V_l = V_{DOPE} + xV_{DOG}, \quad (8)$$

where V_{DOPE} and V_{DOG} are the molecular volumes of the two components. Then all of the recipes and equations provided in Materials, Methods, and Analysis for single-component monolayers can be used without any modification, except that all molecular parameters like molecular area and volume now refer to the effective molecule.

We use normalized areas (A/V_l) and volumes (V/V_l) for the diagnostic A_w^2 versus A_w/R_w plot. Then Eq. 6 can be rewritten in the following form:

$$\frac{A_w^2}{V_l^2} = \frac{A_p^2}{V_l^2} - 2\frac{V_p}{V_l}\frac{A_w}{V_l R_w}. \quad (9)$$

Because A_w/V_l depends only on d_{hex} and ϕ_w, as defined by Eq. 2, and because the relationship between d_{hex} and ϕ_w is independent of the DOG concentration (Fig. 2 *b*), the $(A_w/V_l)^2$ versus A_w/V_lR_w plot must be independent of the DOG concentration.

The $(A_w/V_l)^2$ versus A_w/V_lR_w plots for DOPE and all DOPE/DOG mixtures are pooled in Fig. 4. Linearity of the plots indicates that each mixture has a well-defined pivotal plane. The relative position of the pivotal plane (V_p/V_l) is independent of the DOPE/DOG ratio in the mixture. This is a direct consequence of the fact that in less than excess water the hexagonal dimension for any of the mixtures depends only on the water content, but not on the DOG concentration.

We use a common linear fit of all DOPE/DOG mixtures, as shown in the Fig. 4, to determine the molecular area at the pivotal plane from the intercept ($A_p/V_l \approx 0.0525$ Å^{-1}) and the volume from the slope ($V_p/V_l \approx 0.303$) of the plot. Because these values are independent of DOG concentration, the area per effective molecule at the pivotal plane (A_p) and the polar volume separating the Luzzati and pivotal planes (V_p) increase linearly with the molar ratio x of DOG to DOPE,

$$A_p = A_p^{DOPE} + xA_p^{DOG} \approx 0.0525\ \text{Å}^{-1}(V_{DOPE} + xV_{DOG}), \quad (10)$$

$$V_p = V_p^{DOPE} + xV_p^{DOG} \approx 0.303(V_{DOPE} + xV_{DOG}). \quad (11)$$

Both DOPE and DOG contribute constant molecular areas and volumes, $A_p^{DOPE} \approx 65$ Å^2, $A_p^{DOG} \approx 59$ Å^2, $V_p^{DOPE} \approx 375$

TABLE 2 Structural dimensions derived for the fully hydrated hexagonal phases of various DOPE/DOG mixtures

DOG/DOPE mol ratio	d_{hex} (Å)	V_l (Å^3)	V_w (Å^3)	n_w	R_w (Å)	d_l (Å)	d_m (Å)	d_{lhc} (Å)	d_{mhc} (Å)	A_w (Å^2)	A_t (Å^2)	A_{2hct} (Å^2)
0	63.8	1235	524	17.5	21.1	31.5	42.9	20.4	31.8	49.6	95.4	95.4
0.116	58.1	1364	460	15.3	17.7	31.7	42.1	20.6	31.0	52.0	108.7	97.5
0.173	55.7	1428	430	14.3	16.2	31.8	41.8	20.7	30.6	52.9	115.6	98.5
0.208	54.7	1466	419	14.0	15.6	31.9	41.7	20.7	30.5	53.6	119.4	98.9
0.348	50.5	1624	362	12.1	13.1	32.1	41.2	20.9	29.9	55.4	136.3	101.1

Here d_{hex} is the average first-order x-ray spacing, and V_l is the volume of an effective lipid molecule defined by Eq. 8. V_w and n_w are the volumes and numbers of water molecules per effective molecule. R_w is the radius of the water cylinder. The d spacings are equivalent "bilayer" spacings as defined by Rand and Fuller (1994) and shown in Fig. 1. A_w is the area available per effective molecule on the Luzzati surface. A_t and A_{2hct} are the areas available, per effective molecule and per two hydrocarbons chains respectively, on the surface of the parallel prisms forming the hexagonal packing, a surface effectively populated by the ends of the hydrocarbon chains.

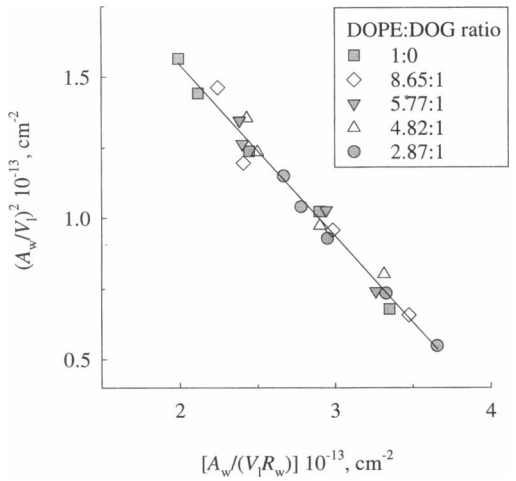

FIGURE 4 Diagnostic plots, as described in Eqs. 6 and 9, relating molecular area at the Luzzati plane A_w with the radius of the water cylinder R_w. When the area is normalized by the volume of an effective molecule (V_l) as described in the text, no systematic variation can be seen with the mole ratio DOG/DOPE. The results were pooled to yield the plotted linear least-squares fit. The slope of this plot ($2V_p/V_l$) defines the fraction of molecular lipid volume included inside the pivotal surface.

Å^3, $V_p^{DOG} \approx 338$ Å^2, all of which are independent of the DOG concentration.

Having determined the value of V_p/V_l from the gravimetric experiments, we use Eq. 5 with R_w and V_p to calculate the radii of curvature at the pivotal plane, R_p, for the osmotic stress experiments. Then following Eq. 7, Fig. 5 shows the ΠR_p^2 versus $1/R_p$ plots for DOPE and five different mixtures of DOPE and DOG, where Π is the osmotic pressure of the equilibrating solution. From the intercepts at $\Pi = 0$ and the slopes of the plots we find the radii of spontaneous curvature (R_{0p}) and the bending moduli (k_{cp}) as

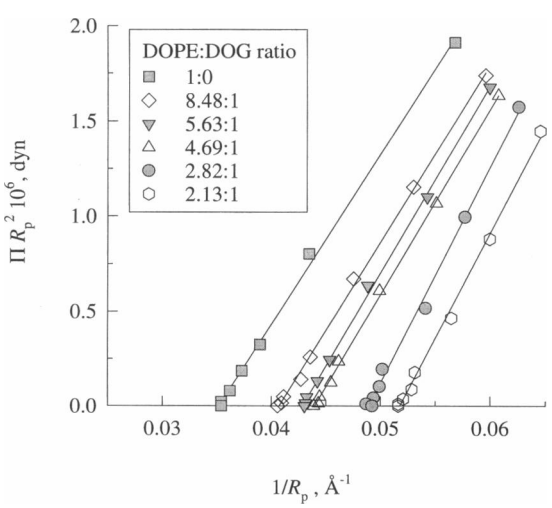

FIGURE 5 "Traditional" (Gruner et al., 1986; Rand et al., 1990) plot to determine, from the stressing pressure Π and radius at the pivotal plane R_p, the intrinsic radius of curvature R_{0p} and bending modulus k_{cp} for hexagonal phase monolayers of increasing mole ratio DOG/DOPE.

defined by Eq. 7. (Within the experimental error, the measurement of the spontaneous curvature from extrapolation of the osmotic stress results gives the same value as the direct but less accurate estimate from structural parameters of the H_{II} phase in excess water. The latter is more prone to experimental error, as indicated by the larger scatter of the data. This is most likely due to some residual stress (osmotic, packing, etc.) or to minor impurities in the lipid.)

The spontaneous curvature $1/R_{0p}$, plotted in Fig. 6, is a linear function of the DOG molar fraction [$m_{DOG} = x/(1 + x)$]:

$$\frac{1}{R_{0p}} = (1 - m_{DOG})\frac{1}{R_{0p}^{DOPE}} + m_{DOG}\left(\frac{1}{R_{0p}^{DOG}}\right). \qquad (12)$$

Apparent specific radii of curvature for each of the components are $R_{0p}^{DOPE} \approx 28.5$ Å and $R_{0p}^{DOG} \approx 11.5$ Å. The dependence of the bending modulus (k_{cp}) on DOG concentration is shown in Fig. 7.

DISCUSSION

Experimental observations

In previous work (Rand and Fuller, 1994) we compiled a variety of structural dimensions of the DOPE hexagonal phase as shown in Fig. 1, and observed how they change both with water content and during the hexagonal-lamellar transition. Table 2 lists these several dimensions, at full hydration, and as they are affected by replacing DOPE with DOG. Remarkably, such replacement results in changes in lattice dimension and structural parameters identical to

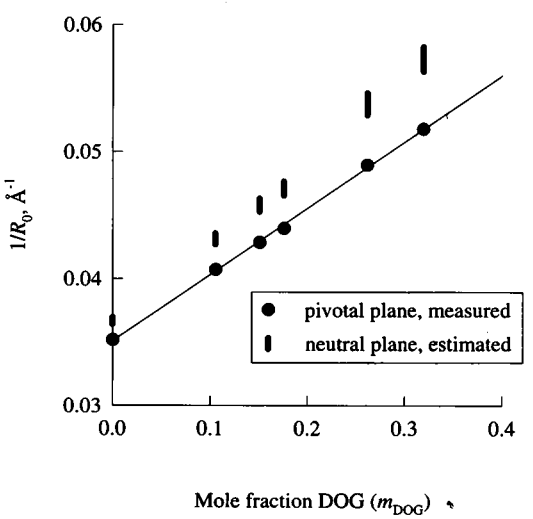

FIGURE 6 Plot of the spontaneous curvature, $1/R_0$, as it varies with increasing mole ratio DOG/DOPE. ●, Values determined at the pivotal plane. The bars illustrate the estimated range for the spontaneous curvature at the neutral surface obtained by solving Eqs. 13–15, with $K = 100$–150 dyn/cm (see Discussion). The large increase in spontaneous curvature with DOG content, although accurately measured only at the pivotal plane, likely applies to other geometries and deformations, like planar membranes, because the estimated change at the neutral surface is very similar.

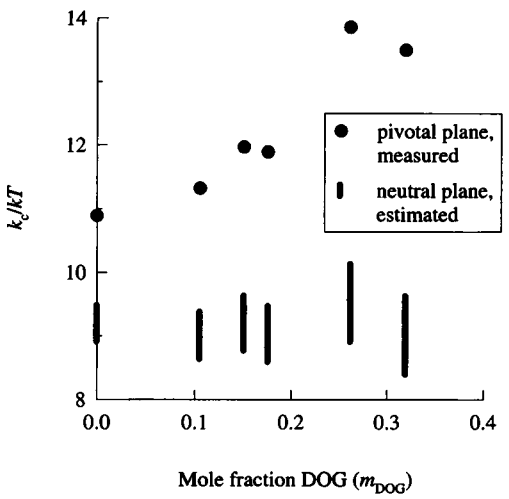

FIGURE 7 Plot of the bending modulus k_c in kT units ($\approx 4.1 \times 10^{-14}$ erg at 25°C), as it varies with increasing mole ratio DOG/DOPE. The values at the pivotal (measured) and neutral (estimated) surfaces are shown by solid circles and bars, correspondingly (see previous figure and Discussion). Unlike spontaneous curvature, the measured increase in pivotal plane bending modulus with DOG content cannot be easily extended to other surfaces and deformations and geometries. Specifically, the estimated bending modulus at the neutral surface remains approximately constant at $\sim 9kT$.

those produced by dehydrating pure DOPE to the same lattice dimension. The hexagonal phase dimension (d_{hex}) at lower than full hydration depends only on the water concentration and does not depend on the DOPE/DOG ratio in the mixture (Fig. 2 *b*).

One is provoked to examine the structural changes that occur with increasing DOG content and to think of mechanical models of the mixed monolayer that would predict this puzzling behavior. We can now restate this problem using the language of elastic deformations. Then the question is, why is the pivotal plane position (V_p/V_l) independent of the DOPE/DOG ratio?

Data analysis

The new diagnostic A_w^2 versus A_w/R_w plot is exquisitely sensitive to the form of the experimental data. Applied to the previous measurements for pure DOPE (Rand et al., 1990), that plot is nonlinear and bends upward instead of bending downward, suggesting that a unique pivotal plane does not exist, and that the approximations of the linear elastic theory (see Appendix) cannot be used for the full set of the older data. However, whereas the osmotic stress data for pure DOPE collected now and before are completely consistent, there is a detectable difference in the gravimetric data, but only close to the full hydration of the lipid, a region most sensitive to experimental control. We do not know the exact source of this discrepancy, but, for example, as little as 1–2% charged lipid could account for it (Lerche et al., 1992). Using the full set of osmotic stress data and the less hydrated older gravimetric data, we now get complete agreement between data sets for the pivotal plane position, the spontaneous curvature, and the bending modulus.

Interpretation of the results

Deformation of a highly curved lipid monolayer can be described by molecular areas and curvatures at either pivotal or neutral planes (Fig. 1), the two most commonly used dividing surfaces (for rigorous definitions see the Appendix). In the tradition of the previous measurements of the H_{II} phase (Rand et al., 1990), we determine the spontaneous curvatures and the bending moduli for the pivotal plane. Even though it works remarkably well, this approach has a serious limitation. The position of the pivotal plane depends on the relationship between area compressibility and bending of the monolayer.

Indeed, for pure changes in area, the pivotal plane does not exist. One may speak of a pivotal plane located at infinite separation from the monolayer. With increasing energetic contribution from bending relative to stretching deformation, the pivotal plane gradually moves toward and into the monolayer until it coincides with the neutral surface. The deformation with coinciding neutral and pivotal surfaces is usually defined as a pure bending deformation.

Hydration of the H_{II} phase is a specific deformation with specific ratio between the bending and stretching. For small changes in curvature we can find a unique position of the pivotal plane, as demonstrated in the Appendix. However, this position as well as the pivotal plane elastic constants are specific to the osmotic and gravimetric hydration of the H_{II} phase. For example, most often bending elasticity is measured for lipid bilayers. For bending deformation of symmetrical bilayers in the absence of bilayer stretching and when the monolayers can freely slide along each other, the pivotal plane coincides with the neutral surface. This is not the case for the H_{II} phase hydration when the neutral and pivotal surfaces are different and have significantly different bending moduli, as shown in the Appendix and discussed below.

Unlike the pivotal plane, the position of the neutral surface does not depend on the deformation or the experimental technique (Kozlov and Winterhalter, 1991b). Furthermore, the spontaneous curvature and bending modulus defined for the neutral plane are unique, intrinsic properties of the lipid (for more detail see the Appendix). However, it is much more difficult to determine the position of the neutral plane in the H_{II} phase. This cannot be done with enough accuracy using the available data. To determine the spontaneous curvature and bending modulus defined for the neutral plane, we use the relationships between the elastic parameters at the pivotal and neutral planes that are derived in the Appendix for small deformations.

The radius of spontaneous curvature at the pivotal plane, R_{0p}, is related to the radius of spontaneous curvature at the neutral plane, R_{0n}, by (see Appendix)

$$R_{0p} = R_{0n}\left(\frac{1+\gamma}{1-\gamma}\right)^{1/2}, \qquad (13)$$

where

$$\gamma = \frac{k_{cn}}{K R_{0n}^2}. \quad (14)$$

K is the lateral compressibility modulus of the monolayer and k_{cn} is the bending modulus defined for the neutral plane. The bending moduli at the neutral (k_{cn}) and at the pivotal (k_{cp}) planes are related by (see Appendix)

$$k_{cp} = \frac{(1+\gamma)^{3/2}}{(1-\gamma)^{5/2}} k_{cn}. \quad (15)$$

If the value of K were measured independently, we could solve these equations and find R_{0n} and k_{cn} from the measured R_{0p} and k_{cp}. Because at the present moment the values of K for DOPE/DOG mixtures are unavailable, we can only estimate the neutral plane elastic parameters.

Using $K \approx 100$–150 dyn/cm (Evans and Needham, 1987) and the measured values of R_{0p} and k_{cp}, we solve Eqs. 13–15 for γ, R_{0n}, and k_{cn}. This estimate shows that γ increases from ~0.03-0.05 in pure DOPE to ~0.08-0.1 with the addition of 30% DOG. The increase in γ is due to the decrease in the radius of spontaneous curvature (Fig. 6). Because γ is a small parameter, we can use simpler relationships between the spontaneous curvatures and the bending moduli:

$$R_{0p} \approx (1+\gamma)R_{0n}, \quad k_{cp} \approx (1+4\gamma)k_{cn}. \quad (16)$$

The difference in spontaneous curvatures between the pivotal and neutral planes is only ~3-10% (depending on the DOG concentration). This difference is small compared to the variation in the spontaneous curvature with the DOPE/DOG ratio. The increase in the spontaneous curvature with DOG content observed here for the pivotal plane, therefore, is also valid for the neutral plane, as shown in Fig. 6. The observed linear change in the spontaneous curvature is consistent with the model of a composite lipid monolayer (Kozlov and Helfrich, 1992) as a simple mixture of components that contribute in proportion to their molar fraction.

The estimated difference between the neutral and pivotal plane bending moduli is not small. It increases from ~15% in pure DOPE to ~40% in the 2.13:1 DOPE/DOG mixture. The bending modulus defined for the neutral plane remains approximately constant (~$9kT$) independent of the DOG concentration (Fig. 7). Keeping in mind that our estimates have some uncertainty due to the unknown lateral rigidity modulus K for DOPE/DOG mixtures, we can only speculate that the neutral surface bending modulus does not change appreciably with DOG. Currently we have no explanation for this puzzling result. However, accepting as given that the monolayer resistance to pure bending remains constant, we can trace back the source of the observed increase in the pivotal plane bending modulus with higher DOG content. Indeed, as the spontaneous curvature increases, the pivotal plane moves away from the neutral surface. Dehydration of the H_{II} phase (bending around the pivotal plane) then requires stronger compression deformation of the neutral surface (in addition to bending) and, as a result, more energy (for more detail see the Appendix).

CONCLUDING REMARKS

DOG is a biologically regulated second messenger that both sensitively affects lipid-protein interactions in membranes and is correlated with the topological changes associated with membrane and bilayer fusion. As a lipid that induces the hexagonal phase, it satisfies those several long-standing speculations concerning the role of hexagonal-prone lipids in membranes. This work attempted to inform those speculations by measuring the specific effects that DOG induces on the physical properties of phospholipid bilayers.

The intrinsic radius of monolayer curvature is significantly reduced by DOG in the hexagonal phase, and we conclude that it would also change, in a similar direction at least, around DOG-containing sites in planar membranes. This argues that such sites favor, or could induce, protein conformations requiring high curvature.

The measurements also show that the bending modulus of hexagonal phase monolayers, deformed by changing hydration and measured at the pivotal plane, increases with increasing DOG content. However, an important lesson of the analysis is that although this measurement represents a real change in bending energy for the hexagonal phase, it was not sufficiently accurate to judge whether the bending modulus changes with DOG content in other geometries and other modes of deformation. We judge that the change if any is small, but what is small for a protein is moot, and the proteins are silent on the issue.

APPENDIX

In this appendix we analyze the deformations that result upon changing the H_{II} phase hydration. We give rigorous definitions for the neutral and pivotal planes, derive the relationships between the spontaneous curvatures and bending moduli defined for these planes, analyze the diagnostic A_w^2 versus A_w/R_w plot, and discuss several other issues associated with the use of these two dividing surfaces.

Gibbs dividing surfaces, the neutral surface

We use traditional definitions of Gibbs dividing surfaces. We start from the lipid/water interface (Luzzati plane), which is a cylinder (Fig. 1) with zero surface excess of material (water and lipid). Obviously, the Luzzati plane lies somewhere in the region of the lipid polar heads. From the Luzzati plane we define other dividing surfaces lying inside the lipid. We neglect volume compressibility of lipid and water, and instead of constant amount of material we speak of constant volume between the dividing surfaces. We define a dividing surface as a cylinder that incorporates a constant volume of lipid (per molecule), V, between this cylinder and the Luzzati plane.

At small deviations from the spontaneous state, the elastic energy per lipid molecule at any of these cylindrical Gibbs dividing surfaces (including the Luzzati plane) has the form (Kozlov and Winterhalter, 1991b)

$$F \approx \frac{1}{2} A_0 E_{RR}\left(\frac{1}{R} - \frac{1}{R_0}\right)^2 + E_{AR}(A - A_0)\left(\frac{1}{R} - \frac{1}{R_0}\right) + \frac{1}{2} E_{AA}\frac{(A-A_0)^2}{A_0}, \quad (A.1)$$

which is just a quadratic expansion of the free energy with respect to deviation of the curvature, $1/R$, and area per lipid molecule, A, from their spontaneous (intrinsic) values, $1/R_0$ and A_0. The values of the elastic moduli (E_{RR}, E_{AR}, and E_{AA}) and the dimensions (R and A) depend on the selection of the dividing surface. The dimensions for two different dividing surfaces are related by Eqs. 4 and 5. General equations relating the elastic moduli are given by Kozlov and Winterhalter (1991b).

It is most convenient to analyze deformation of the H_{II} phase using the dimensions at the neutral surface. This is a special dividing surface where the cross-coefficient E_{AR} is exactly zero (Kozlov and Winterhalter, 1991b), i.e., the elastic energy/molecule,

$$F \approx \frac{1}{2} A_{0n} k_{cn} \left(\frac{1}{R_n} - \frac{1}{R_{0n}} \right)^2 + \frac{1}{2} K \frac{(A_n - A_{0n})^2}{A_{0n}}, \qquad (A.2)$$

is described by only two elastic moduli of bending (k_{cn}) and stretching (K). The position of the neutral surface is determined only by the mechanical properties of the lipid and is independent of the deformation as long as the elastic response remains linear.

Deformation of the neutral surface upon hydration

The experimental techniques used in this work define a certain type of H_{II} phase deformation. The dimensions of the H_{II} phase are regulated by the amount of water per lipid, which is either fixed by gravimetric mixing or controlled osmotically. Most of the following derivations are valid only for this type of the deformation and are specific for the gravimetric and osmotic measurements of the H_{II} phase hydration.

This deformation can be characterized by the relationship between the molecular area A_n and the radius of curvature R_n of the neutral surface. From simple geometrical considerations we find that A_n and R_n are related by

$$R_n A_n = 2V_n + 2V_l \frac{\phi_w}{1 - \phi_w}, \qquad (A.3)$$

where ϕ_w is the volume fraction of water in the lipid/water mixture, V_n is the volume (per lipid molecule) between the Luzzati and neutral planes, and V_l is the molecular volume of the lipid. In thermodynamic equilibrium the elastic energy of the H_{II} phase must be minimal with respect to A_n variation at constant ϕ_w, i.e.,

$$\left(\frac{\partial F(R_n, A_n)}{\partial A_n} \right)_{\phi_w} = \frac{\partial F(R_n, A_n)}{\partial A_n} + \left(\frac{\partial F(R_n, A_n)}{\partial R_n} \right)_{A_n} \left(\frac{\partial R_n}{\partial A_n} \right)_{\phi_w} = 0. \qquad (A.4)$$

By solving Eqs. A.3 and A.4 together we can either express A_n and R_n as functions of ϕ_w or determine the relationship between A_n and R_n. It follows from Eq. A.3 that

$$\left(\frac{\partial R_n}{\partial A_n} \right)_{\phi_w} = -\frac{R_n}{A_n}. \qquad (A.5)$$

Substituting Eq. A.5 into Eq. A.4, we find

$$A_n \approx A_{0n} \left(1 - \gamma R_{0n} \left(\frac{1}{R_n} - \frac{1}{R_{0n}} \right) \right), \qquad (A.6)$$

where

$$\gamma = \frac{k_{cn}}{K R_{0n}^2}. \qquad (A.7)$$

Note that in Eq. A.6 we retained only the first-order terms in the curvature change. This is because Eq. A.1 is an expansion of the free energy up to the second-order terms. Because a third-order term in Eq. A.1 would contribute to a second-order term in Eq. A.6, the latter must be omitted so that we do not exceed the accuracy of the initial approximation.

The pivotal plane

In keeping with the tradition set by osmotic stress measurements of the H_{II} phase (Rand et al., 1990), we define the pivotal plane as a cylindrical Gibbs dividing surface associated with a specific place inside the lipid (so that V_p does not change upon hydration) where the molecular area, A_p, remains constant. The pivotal plane always exists for small deformations near the spontaneous state. Mathematically it can be defined as the plane where

$$\left. \frac{\partial A_p}{\partial R_n} \right|_{R_n = R_{0n}} = 0. \qquad (A.8)$$

From Eq. A.8 and Eq. A.1 we find that the pivotal plane elastic energy is the energy of bending,

$$F \approx \frac{1}{2} A_p k_{cp} \left(\frac{1}{R_p} - \frac{1}{R_{0p}} \right)^2. \qquad (A.9)$$

To find the location of the pivotal plane (V_p), we make use of the fact that the molecular areas at the neutral and pivotal planes are related by Eq. 4, which is valid for any two dividing surfaces and can be rewritten in the form

$$A_p^2 = A_n^2 + 2(V_p - V_n) \frac{A_n}{R_n}, \qquad (A.10)$$

where V_p is the volume between the Luzzati and pivotal planes and $V_p - V_n$ is the volume between the neutral and pivotal planes. Substituting this and Eq. A.6 into Eq. A.8 and solving for V_p, we obtain

$$V_p = V_n + A_{0n} R_{0n} \frac{\gamma}{1 - \gamma}. \qquad (A.11)$$

From Eqs. A.6, A.8, and A.11 and using the relation $A_p/R_p = A_n/R_n$, we find the radius of spontaneous curvature and the molecular area at the pivotal plane,

$$R_{0p} = R_{0n} \left(\frac{1 + \gamma}{1 - \gamma} \right)^{1/2} \qquad (A.12)$$

and

$$A_p \approx A_{0n} \left(\frac{1 + \gamma}{1 - \gamma} \right)^{1/2}. \qquad (A.13)$$

In Eq. A.13 we omit the second-order and higher order terms in the curvature change so that we do not exceed the accuracy of the initial approximation, as in the derivation of Eq. A.6. For small deformations A_p is independent of the curvature.

To find the relationship between the bending moduli at the pivotal (k_{cp}) and neutral (k_{cn}) planes we rewrite Eq. A.9 by substituting the area, radius of curvature, and spontaneous radius of curvature at the neutral plane (A_{0n}, R_n, and R_{0n}) instead of the area and radii at the pivotal plane (A_p, R_p, and R_{0p}),

$$F \approx \frac{1}{2} A_{0n} k_{cp} \frac{(1 - \gamma)^{5/2}}{(1 + \gamma)^{1/2}} \left(\frac{1}{R_n} - \frac{1}{R_{0n}} \right)^2. \qquad (A.14)$$

On the other hand, substituting Eq. A.6 into Eq. A.2, we find

$$F \approx \frac{1}{2} A_{0n} k_{cn} (1 + \gamma) \left(\frac{1}{R_n} - \frac{1}{R_{0n}} \right)^2. \qquad (A.15)$$

Comparing these two equations, we obtain

$$k_{cp} = \frac{(1+\gamma)^{3/2}}{(1-\gamma)^{5/2}} k_{cn}. \qquad (A.16)$$

Large curvature changes

Strictly speaking, the neutral and pivotal planes are well defined only for small deformations within the limits of validity of the quadratic free energy expansion (Eq. A.1). In the experiment, however, the curvature changes by up to a factor of 2. Still, the data can be described surprisingly well using the pivotal plane approximation with linear elastic response. The following is an attempt to explain possible reasons for this.

Consider the approximation of linear elastic response, Eq. A.1, for large curvature changes. In other words, instead of using Eq. A.1 as a quadratic expansion of the free energy that is valid for small deformations only, we use it as the free energy for all deformations. Then we must retain all terms in the calculation of the molecular areas. We cannot omit high-order terms with respect to the curvature change, unlike what we have done above.

Then, instead of Eq. A.6, we find

$$A_n = A_{0n}\left(\frac{1}{2} + \frac{1}{2}\sqrt{1 - 4\gamma\frac{R_{0n}(R_{0n}-R_n)}{R_n^2}}\right), \qquad (A.17)$$

and instead of Eq. A.13 we get

$$A_p \approx A_{0n}\left[1 + \gamma\left(1 - \frac{(R_{0n}-R_n)^2}{R_n^2}\right)\right], \qquad (A.18)$$

where, for simplicity, we show only the first-order term with respect to γ (the expected value of γ is $\gamma \approx 0.1$ or even smaller; see below and the Discussion).

From Eq. A.18 we see that the molecular area at the dividing surface defined by Eq. A.5 changes. A true pivotal plane that incorporates constant lipid volume and retains constant molecular area at large deformations does not exist unless $\gamma = 0$. Then why does the measured diagnostic A_w^2 versus A_w/R_w plot remain linear in the full range of the curvatures? The linearity of this plot indicates that a well-defined pivotal plane (with constant molecular area) exists.

The diagnostic plot

To answer this question, we compare the measured A_w^2 versus A_w/R_w plot (Fig. 4) with the one calculated assuming the linear elastic response at large curvature changes. Fig. 8 shows the calculated normalized $(A_w/V_l)^2$ versus A_w/V_lR_w plot for different values of γ. To calculate A_w and R_w we use the relations

$$A_w^2 = A_n^2 - 2V_n\frac{A_n}{R_n} \quad \text{and} \quad \frac{A_w}{R_w} = \frac{A_n}{R_n}, \qquad (A.19)$$

where $A_n(R_n)$ is given by Eq. A.17, $V_n/V_l = 0.3$, and $R_{0n} = 30$ Å.

At infinite stretching rigidity K of the monolayer ($\gamma \to 0$) the plot is linear. In this case the neutral surface does not change its area and becomes the pivotal plane. This would be the simplest explanation for the data if it did not contradict the existing knowledge. We estimate that the area change at the neutral surface becomes negligible compared to the experimental error at $K > 500$ dyn/cm. The estimate of K based on the values measured (Evans and Needham, 1987) for a number of different phospholipid bilayers is $K \approx 100$–150 dyn/cm. In principle, the local lateral rigidity in the H_{II} phase might be higher than the macroscopic rigidity measured in large bilayer vesicles. Still, until this is experimentally demonstrated we have to consider this explanation to be inconsistent.

Using more consistent values for $K \approx 100$–150 dyn/cm, we estimate $\gamma \approx 0.03$–0.1 depending on the DOG concentration (see Discussion). The

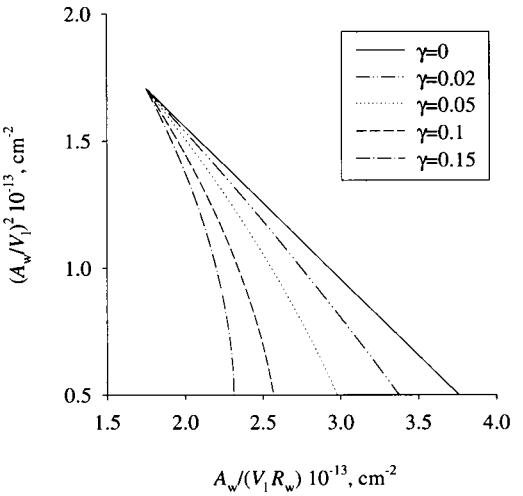

FIGURE 8 Theoretical plots for an idealized linear elastic response showing the dependence of the linearity of diagnostic plot on $\gamma = k_{cn}/KR_{0n}^2$. The plots were calculated from Eq. A.19 as described in the text, assuming that $A_{0n}/V_l = 0.53$, $V_n/V_l = 0.3$, and $R_{0n} = 30$ Å. With increasing γ the plots bend downward and become more nonlinear.

calculated diagnostic plot at $\gamma \approx 0.03$–0.1 (Fig. 8) is not a straight line: it bends downward. However, if we compare the deviation with the experimental error, it may be experimentally indistinguishable from a straight line. In other words, even though the curvature change is large, the experimental error may make the associated corrections invisible. With the same accuracy as dictated by the data, we can still use the simple definition of the pivotal plane and the simple relations between the spontaneous curvatures and between the bending moduli at the pivotal and neutral planes derived for the small deformations limit. We base our interpretation of the experimental results on this assumption.

Note that we cannot exclude the possibility that the diagnostic plot linearity at large curvature changes reflects a nonlinear elastic response of the lipid. As we have already mentioned, the second-order and higher order terms in A_n and A_p with respect to the curvature variation are affected by the third-order and higher order terms in the free energy expansion. In principle, mutual compensations of the second-order and higher order corrections to A_p may create a well-defined pivotal plane. The elastic response to bending relative to this plane may then only appear linear. There is no experimental evidence, however, for this interpretation of the DOPE/DOG data.

H_{II} phase-specific elasticity

As we have discussed, the pivotal plane position and elastic constants are specific to a particular deformation. The elastic parameters we have measured are valid only for the osmotic or gravimetric dehydration of the H_{II} phase. A more universal description would be based on a neutral surface of bending. The neutral surface elastic constants are intrinsic mechanical properties of lipid monolayers. They remain the same for any small deformation. This difference between the neutral and pivotal surfaces is well illustrated by the dependence of the bending rigidity on DOG concentration in DOG/DOPE mixtures, shown in Fig. 7. Whereas the intrinsic bending rigidity is practically independent of the mixture composition, the measured pivotal plane bending modulus increases with DOG. This is because the osmotic (or gravimetric) dehydration of the H_{II} phase requires stronger compression of the neutral surface at higher spontaneous curvature. The compression/bending ratio, characterized by the parameter γ, increases quadratically with the spontaneous curvature.

Deformation-independent neutral surface elastic constants may still be H_{II}-phase-specific because of H_{II}-phase-specific elastic forces like those

associated with hexagonal interstices ("voids" in hexagonal lipid packing). The elastic theory discussed here implicitly accounts for the interstices as well as for all other H_{II}-phase-specific forces simply because Eq. A.1 is just a quadratic expansion of the total free energy, which includes all of the curvature-dependent contributions. Provided that the energy of the interstices would be curvature dependent, they would contribute to the elastic constants in Eq. A.1. Then the position and elastic parameters of the neutral surface would be H_{II}-phase-specific. Although this is a plausible scenario, it is not supported by a model for the interstices suggested and justified by Siegel (1993). When written in terms of Eq. A.1, this model gives a curvature-independent energy of the interstices for small deviations from the spontaneous curvature, so that the neutral surface retains its universality. We believe, though, that this issue should not be considered closed until sufficient experimental evidence is found.

Even when not important for small deformations, the H_{II}-phase-specific forces may become significant at large deformations associated with big changes in the H_{II} phase structural parameters. For example, nonlinearity of the elastic response associated with the interstices may be one of the mutually compensating factors discussed above that ensure apparent linearity of the diagnostic plot at large curvature changes. Again, in the absence of experimental evidence this question remains open.

We thank Wolfgang Helfrich and Adrian Parsegian for many fruitful discussions.

This work was supported by a research grant from the Natural Science and Engineering Research Council of Canada to RPR and by a Deutsche Forschungsgemeinschaft grant He 952/15-1 to MMK. MMK and RPR acknowledge financial support during a visit to the Laboratory of Structural Biology, Division of Computer Research and Technology, National Institutes of Health. This work was undertaken when RPR was a Killam Research Fellow of the Canada Council.

REFERENCES

Allan, D., and R. H. Michell. 1975. Accumulation of 1,2-diacylglycerol in the plasma membrane may lead to echinocyte transformation of erythrocytes. *Nature.* 258:348–349.

Berridge, M. J. 1984. Inositol and diacylglycerol as second messengers. *Biochem. J.* 220:345–360.

Das, S., and R. P. Rand. 1986. Modification by diacylglycerol of the structure and interaction of various phospholipid bilayer membranes. *Biochemistry.* 25:2882–2889.

Dawson, R. M. C., R. F. Irvine, J. Bray, and P. J. Quinn. 1984. Long-chain unsaturated diacylglycerols cause a perturbation in the structure of phospholipid bilayers rendering them suscepitible to phospholipase attack. *Biochem. Biophys. Res. Commun.* 125:836–842.

Evans, E., and D. Needham. 1987. Physical properties of surfactant bilayer membranes: thermal transitions, elasticity, rigidity, cohesion, and colloidal interactions. *J. Phys. Chem.* 91:4219–4228.

Goldberg, E. M., D. S. Lester, D. B. Borchardt, and R. Zidovetzki. 1994. Effects of diacylglycerols and Ca on structure of phosphatidylcholine/phosphatidylserine bilayers. *Biophys. J.* 66:382–393.

Goldberg, E. M., D. S. Lester, D. B. Borchardt, and R. Zidovetzki. 1995. Effects of diacylglycerols on conformation of phosphatidylcholine headgroups in phosphatidylcholine/phosphatidylserine bilayers. *Biophys. J.* 69:965–973.

Gruner, S. M., V. A. Parsegian, and R. P. Rand. 1986. Directly measured deformation energy of phospholipid H_{II} hexagonal phases. *Faraday Discuss. Chem. Soc.* 81:29–37.

Helfrich, W. 1973. Elastic properties of lipid bilayers: theory and possible experiments. *Z. Naturforsch.* 28C:693–703.

Kirk, G. L., S. M. Gruner, and D. L. Stein. 1984. A thermodynamic model of the lamellar to inverse hexagonal phase transition of lipid membrane-water system. *Biochemistry.* 23:1093–1102.

Kozlov, M. M., and W. Helfrich. 1992. Effects of a cosurfactant on the stretching and bending elasticities of a surfactant monolayer. *Langmuir.* 8:2792–2797.

Kozlov, M. M., and M. Winterhalter. 1991a. Elastic moduli for strongly curved monolayers. Analysis of experimental results. *J. Phys. France II.* 1:1085–1100.

Kozlov, M. M., and M. Winterhalter. 1991b. Elastic moduli for strongly curved monolayers. Position of the neutral surface. *J. Phys. France II.* 1:1077–1084.

Lerche, D., N. L. Fuller, and R. P. Rand. 1992. Membrane curvature and structural transitions for charged/uncharged phospholipid mixtures. *In* The Structure and Conformation of Amphiphilic Membranes. R. Lipowsky, D. Richter, and K. Kremer, editors. Springer-Verlag, Berlin. 226–229.

Lide, D. R., editor. 1994. CRC Handbook of Chemistry and Physics. CRC Press, Boca Raton, FL.

Luzzati, V., and F. Husson. 1962. X-ray diffraction studies of lipid-water systems. *J. Cell. Biol.* 12:207–219.

Nieva, J. L., A. Alonso, G. Basanez, F. M. Goni, A. Gulik, R. Vargas, and V. Luzzati. 1995. Topological properties of two cubic phases of a phospholipid:cholesterol:diacylglycerol aqueous system and their possible implications in the phospholipase C-induced liposome fusion. *FEBS Lett.* 368:143–147.

Nishizuka, Y. 1984. The role of protein kinase C in cell surface signal transduction and tumour promotion. *Nature.* 308:693–698.

Rand, R. P., and N. L. Fuller. 1994. Structural dimensions and their changes in a reentrant hexagonal-lamellar transition of phospholipids. *Biophys. J.* 66:2127–2138.

Rand, R. P., N. L. Fuller, S. M. Gruner, and V. A. Parsegian. 1990. Membrane curvature, lipid segregation, and structural transitions for phospholipids under dual-solvent stress. *Biochemistry.* 29:76–87.

Rand, R. P., and V. A. Parsegian. 1989. Hydration forces between phospholipid bilayers. *Biochim. Biophys. Acta.* 988:351–376.

Siegel, D. P. 1993. Energetics of intermediates in membrane fusion: comparison of stalk and inverted micellar intermediate mechanisms. *Biophys. J.* 65:2124–2236.

Turner, D. C., and S. M. Gruner. 1992. X-ray diffraction reconstruction of the inverted hexagonal (H_{II}) phase in lipid-water systems. *Biochemistry.* 31:1340–1355.

Wakelam, M. J. O. 1983. Inositol phospholipid metabolism and myoblast fusion. *Biochem. J.* 214:77–82.

Whitaker, M., and M. Aitchison. 1985. Ca-dependent polyphosphoinositide hydrolysis is associated with exocytosis in vitro. *FEBS Lett.* 182: 119–124.